ACS OMEGA

Article

Cite This: ACS Omega 2018, 3, 16377−16385

http://pubs.acs.org/journal/acsodf

Fur-Imine-Functionalized Graphene Oxide-Immobilized Copper Oxide Nanoparticle Catalyst for the Synthesis of Xanthene Derivatives

Subodh, Navin Kumar Mogha, Karan Chaudhary, Gyanendra Kumar, and Dhanraj T. Masram*

Department of Chemistry, University of Delhi, Delhi 110007, India

Supporting Information

ABSTRACT: Fur-imine-functionalized graphene oxide-immobilized copper oxide nanoparticles (Cu(II)-Fur-APTES/GO) are synthesized and found to be a cost-effective, efficient, and reusable heterogeneous nanocatalyst for the preparation of pharmaceutically important xanthene derivatives under greener solvent conditions. Cu(II)-Fur-APTES/GO exhibits excellent result in the synthesis of xanthenes with reduced reaction time (25−50 min) and higher yields (up to 95%) and has a simple procedure, ease of product separation, and no byproducts. Moreover, the nanocatalyst has a Cu loading of 13.5 at. % over functionalized GO which is far superior than the already known metal-based heterogeneous catalysts. The newly synthesized catalyst has been characterized by various physiochemical techniques such as X-ray photoelectron spectroscopy, X-ray diffraction, energy-dispersive X-ray, Raman spectroscopy for structural characterization, field emission scanning electron microscopy and high-resolution transmission electron microscopy for morphological characterization. The catalyst showed admirable recyclability up to five consecutive runs, and there was no appreciable loss in catalytic efficiency.

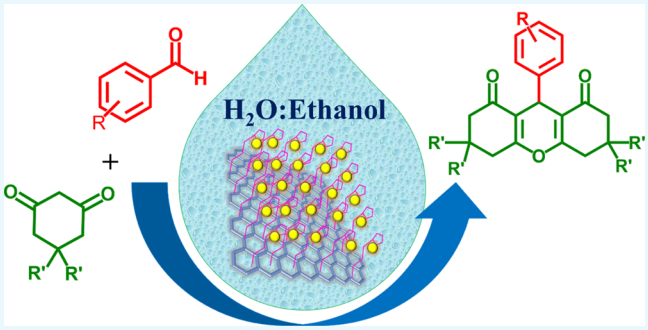

1. INTRODUCTION

Xanthenes have been classified as oxygen-containing molecular families, found in natural products, synthetic bioactive substances, and fluorescent dyes.[1] The core structure of xanthene exhibits a variety of physicochemical and pharmacological properties such as antiviral,[2] antibacterial,[3] analgesic,[3] antimalarial,[4] antiinflammatory,[5] and anticancer.[6] Extensive literature survey has devoted for various routes for the synthesis of xanthenes, for example, sulfamic acid,[7] pTSA,[8] silica sulfuric acid,[9] molecular iodine,[10] $TiO_2-SO_4^{2-}$,[11] $NaHSO_4-SiO_2$,[12] et cyanuric chloride,[13] amberlyst-15,[14] acyclic acidic ionic liquids,[15] core/shell Fe_3O_4@GA@isinglass,[16] and boric acid.[17] However, such a type of catalysts possesses some disadvantages like prolonged work up, harsh reaction conditions, toxic solvents, sluggish and low reaction yields, and so forth, which demands for further development of a novel catalyst for xanthene synthesis with an easy, cost-effective, energy-efficient, and greener method.

The advanced progress of nanocatalysts in various organic transformations got ample attention.[18,19] However, the major problems with nanocatalysts are their recovery and reusability. Therefore, a heterogeneous nanocatalyst can address this problem as they can be easily separated by different filtrations or centrifugation techniques. Graphene, an allotrope of carbon, is one of the extensively investigated 2D materials as the catalyst or support to various metal nanocatalysts exhibiting excellent catalytic activity for different types of organic transformations.[20,22] Graphene and graphene oxide (GO) have excellent mechanical strength, electron transport properties, large specific surface area, good adsorption capacity, high chemical, and thermal stability.[21−23] GO and its nanocomposites have a wide range of applications as catalysts,[24−29] photocatalysts,[30−32] energy storage,[33] sensors,[34−36] hydrogen storage,[37] drug delivery,[38] biomedical devices,[39] supercapacitors,[40,41] and waste water treatment.[42,43] In the backdrop of their excellent synergistic action, GO-based nanocatalysts are rationalized using nanoparticles (NPs) adorning its surface for them to be used as heterogeneous catalysts to overcome different economic and environmental problems.[44] However, metal NPs over a solid support of GO are unstable because of their high surface energy, which leads to irreversible agglomeration and thus reduces the catalytic activity.[45] In order to tackle this problem, silica modification of GO worked as an outstanding protection strategy which prevents the agglomeration of metal NPs and improves catalytic activity.[46] Additionally, chemical modification of GO by imine-functionalized silica increases surface donor sites which bind strongly with metal cations at the surface of the catalyst, thus minimizing the possibility of active metal sites leaching from the catalyst surface.[47] In this article, we report for the first time the synthesis of a new furfural (Fur) imine-functionalized APTES grafted GO nanocatalyst immobilized with copper

Received: July 26, 2018
Accepted: October 29, 2018
Published: November 30, 2018

DOI: 10.1021/acsomega.8b01781
ACS Omega 2018, 3, 16377−16385

Scheme 1. Schematic Diagram Showing Synthetic Procedure of Cu(II)-Fur-APTES/GO

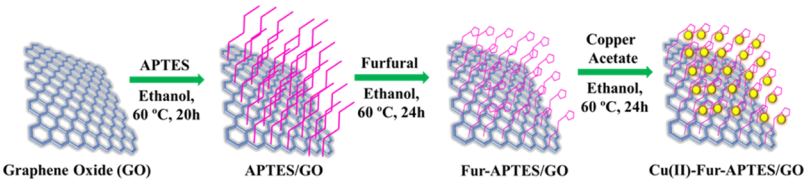

oxide NPs and its efficient catalytic activity for one-pot synthesis of xanthene derivatives under greener solvent conditions. A schematic diagram showing the synthetic procedure of Cu(II)-Fur-APTES/GO is illustrated in Scheme 1.

2. RESULTS AND DISCUSSION

2.1. X-ray Diffraction and Raman Studies. The crystallographic structure and chemical composition of the so formed GO, APTES/GO, Cu(II)-Fur-APTES/GO, and recovered Cu(II)-Fur-APTES/GO were determined by X-ray diffraction (XRD) analysis and XRD patterns are shown in Figure 1i. GO shows its characteristic peaks at 2Θ = 10.3

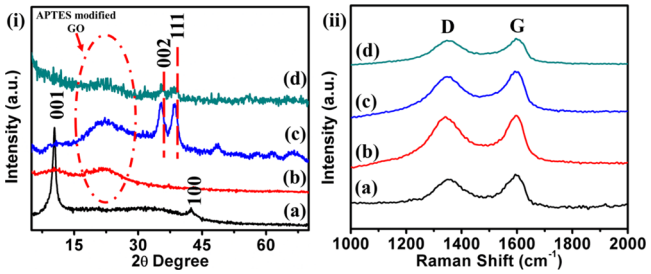

Figure 1. (i) Powder XRD pattern of and (ii) Raman spectra of (a) GO, (b) APTES/GO, (c) Cu(II)-Fur-APTES/GO, and (d) recovered the Cu(II)-Fur-APTES/GO nanocatalyst.

attributing to plane ⟨001⟩ and at 2Θ = 42.5 representing the ⟨100⟩ plane. Furthermore, the XRD pattern of fresh Cu(II)-Fur-APTES/GO and recovered Cu(II)-Fur-APTES/GO after catalysis show peaks at 2Θ = 35.3 and 38.47 attributing to plane ⟨002⟩ and ⟨111⟩ of CuO, respectively, which is in correlation with the literature values.[48] Peak at 2Θ = 10.3 in the XRD pattern disappeared owing to functionalization of APTES on GO along with conversion of GO to reduced GO and a very broad pattern is observed around 2Θ = 22.[49] Raman spectra for GO, APTES/GO, fresh Cu(II)-Fur-APTES/GO, and recovered Cu(II)-Fur-APTES/GO catalyst are shown in Figure 1ii depicting the characteristic D and G band of graphene. The D band of graphene is because of the breathing mode of sp^3-bonded carbon A_{1g} symmetry *j*-point phonons in disordered graphene, whereas the G band represents sp^2-bonded carbon atom associated first order scattering of E_{2g} phonons.The Raman spectrum for GO displayed D and G bands at 1350 and 1594 cm^{-1}, respectively. Similarly, the D band for APTES/GO, fresh Cu(II)-Fur-APTES/GO, and recovered Cu(II)-Fur-APTES/GO has been observed at 1341, 1347, and 1347 cm^{-1}, respectively, whereas the G band appeared at 1596, 1595, and 1596 cm^{-1}, respectively. The I_D/I_G ratio that is, the intensity ratio of D and G bands reflects the disorderness of graphitic carbon in the nanocatalyst. In the present case, the I_D/I_G ratio for GO, APTES/GO, fresh Cu(II)-Fur-APTES/GO, and recovered Cu(II)-Fur-APTES/GO nanocatalyst is found to be 0.89, 0.98, 0.97, and 0.98, respectively. Increment in the I_D/I_G ratio from GO to APTES/GO indicates increase in the sp^3 character of the graphitic carbon, whereas no significant changes observed for the I_D/I_G ratio for Cu(II)-Fur-APTES/GO. This suggest that further modifications of the catalyst have been observed at APTES not at graphitic carbon of GO. Moreover, XRD and Raman characterization suggest that the nanocatalyst shows no significant structural change after catalytic activity.

2.2. Field Emission-Scanning Electron Microscopy. Figure 2 depicts the field emission scanning electron

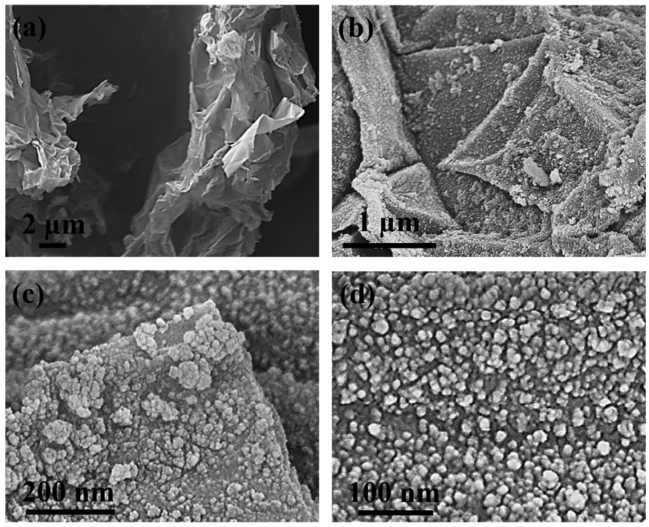

Figure 2. FESEM micrographs of (a) GO, (b–d) Cu(II)-Fur-APTES/GO under different magnification.

microscopy (FESEM) micrographs of GO and Cu(II)-Fur-APTES/GO for detailed analysis of the nanocatalyst surface. Figure 2a, shows the wrinkled sheet-like characteristic morphology of GO, while Figure 2b–d shows the morphology of the Cu(II)-Fur-APTES/GO nanocatalyst under different magnifications. Irregular-shaped NPs of CuO attached to the surface of APTES modified GO has been viewed in these micrographs.

Figure 3 represents the colored elemental mapping images of the Cu(II)-Fur-APTES/GO nanocatalyst surface, different colors indicating the presence of different elements. The energy-dispersive X-ray (EDX) pattern of Cu(II)-Fur-APTES/GO is shown in Figure S1 that confirmed the presence of Cu and Si in the Cu(II)-Fur-APTES/GO nanocatalyst. Figure 3f shows the elemental percentage of Cu(II)-Fur-APTES/GO which was obtained from the EDX pattern. The copper content in Cu(II)-Fur-APTES/GO was detected to be 13.5 at. % by EDX, a far better loading amount than already known in literature[50−56] which is responsible for acting as an efficient catalyst for xanthene synthesis.

DOI: 10.1021/acsomega.8b01781
ACS Omega 2018, 3, 16377−16385

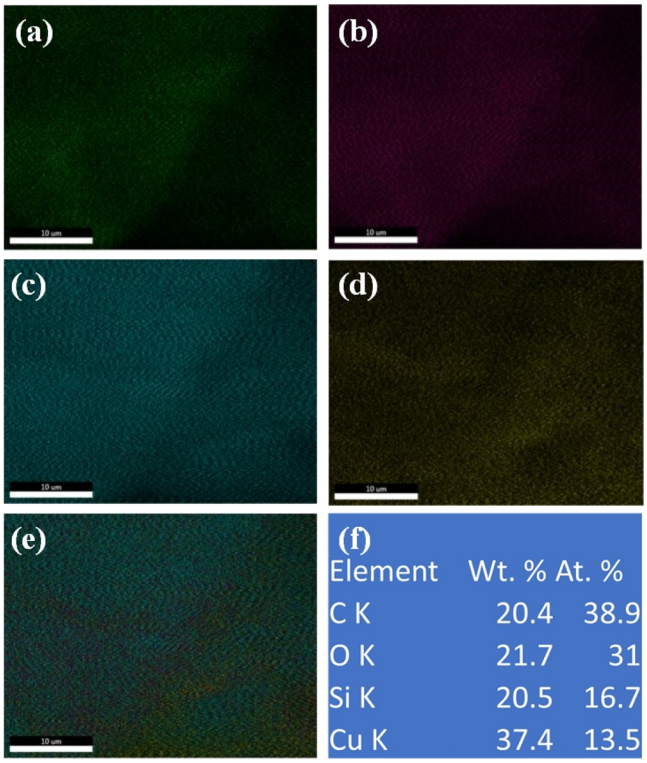

Figure 3. Elemental mapping of (a) carbon (b) oxygen (c) silicon (d) copper (e) combined (f) element percentage table from EDX.

2.3. Transmission Electron Microscopy. GO, fresh Cu(II)-Fur-APTES/GO, and recovered Cu(II)-Fur-APTES/GO were subjected to high resolution transmission electron microscopy (HRTEM) and are illustrated in Figure 4. Figure 4a shows the overlapped sheet-like morphology of GO. Figure 4b,c represent the uniform distribution of CuO NPs in the Cu(II)-Fur-APTES/GO nanocatalyst, under different magnifications. Furthermore, the HRTEM image of the recovered Cu(II)-Fur-APTES/GO nanocatalyst is depicted in Figure 4d, showing no significant change from Figure 4c. These results confirmed that there is no agglomeration of small size CuO NPs in the nanocatalyst after catalysis.

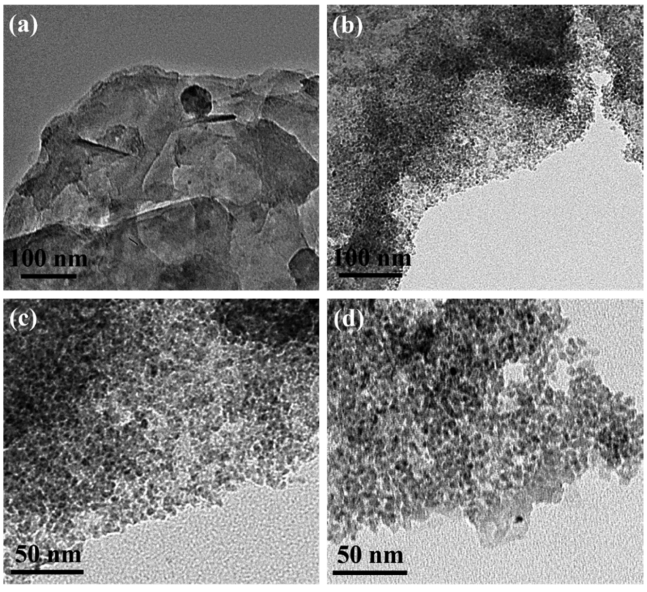

Figure 4. HRTEM micrographs of (a) GO, (b,c) fresh Cu(II)-Fur-APTES/GO nanocatalyst, and (d) recovered Cu(II)-Fur-APTES/GO nanocatalyst.

2.4. X-ray Photoelectron Spectroscopy. Figure 5 shows the X-ray photoelectron spectroscopy (XPS) spectrum of the Cu(II)-Fur-APTES/GO catalyst and peaks at B.E. 283.40 and 286.56 eV can be assigned to C−O−C/C−OH and C═C, respectively, while a band at 101.11 eV attributed to Si−O emerged in the Si 2p spectrum, indicating silylation of the reaction surface. The O 1s peak with B.E. 529.83 eV represents bonding between O^{2-} ions and Cu. The N 1s XPS spectrum reveals that a significant amount of N−H was transformed into N═C (398.35 eV) and the N−H band at 400.24 eV. The Cu 2p XPS spectrum of Cu(II)-Fur-APTES/GO shows two bands at 952.44 and 932.52 eV which corresponds to the bonding energy of Cu $2p_{1/2}$ and Cu $2p_{3/2}$. Meanwhile, a Cu $2p_{3/2}$ and Cu $2p_{1/2}$ satellite peaks were observed at 942.10 and 960.96 eV, respectively.

2.5. Catalytic Activity Test. The catalytic ability of the newly synthesized Cu(II)-Fur-APTES/GO nanocatalyst was investigated by the synthesis of substituted xanthenes. Moreover, to achieve best reaction conditions for the xanthene synthesis, the effect of different significant constraints such as the catalyst amount, reaction time, optimal temperature, and ideal solvent is thoroughly investigated. A model reaction between 5,5-dimethyl-1,3-cyclohexanedione and benzaldehyde is monitored for optimization of these parameters. For comparison purpose, Cu (II)-APTES/GO has shown lesser activity (67% yield for model reaction) as compared to Cu(II)-Fur-APTES/GO because of lesser loading of CuO NPs as observed from the EDX data, Table S3.

2.5.1. Effect of Catalyst Amount, Temperature, Time, and Solvent System. To optimize reaction conditions such as catalytic amount, temperature, and time required for the synthesis of xanthenes, Table 1 demonstrates the varying amounts of Cu(II)-Fur-APTES/GO, temperature range and the time required for the completion of the reaction. First, the effect of the amount of the nanocatalyst, that is, Cu(II)-Fur-APTES/GO is tested with model reaction.

By intensifying the amount of the catalyst up to 20 mg exhibits a noteworthy alteration in the percentage yield. Though, an additional increment in the catalyst amount up to 30 mg, resulted in no change in the conversion percentage. This may be because of the exhaustion of the catalytic site or attainment of the maximum conversion efficiency of the nanocatalyst. Congruently, temperature and time also play an important role in affecting reaction kinetics to large extents. Henceforth, with the intention of studying the effect of these two constraints, a varied range of temperature (25−70 °C) is used to carry out model reaction for different time periods (30−120 min) and by using 20 mg of the nanocatalyst at 50 °C for a reaction time of 30 min the percentage yield (95%) which was found as maximum. It has been observed that no significant change has been observed after prolonged reaction time and increased temperature.

Similarly, even solvents may disturb the reaction environment by changing solubility, stability of catalyst and reactants, and rate of reaction. Therefore, an appropriate choice of solvent can eliminate such disturbances. With the purpose of obtaining an excellent catalytic conversion rate for synthesis of xanthenes, different solvents and solvent mixtures were tested. Figure 6a and Table S1, summarizes the result of variety of

DOI: 10.1021/acsomega.8b01781
ACS Omega 2018, 3, 16377−16385

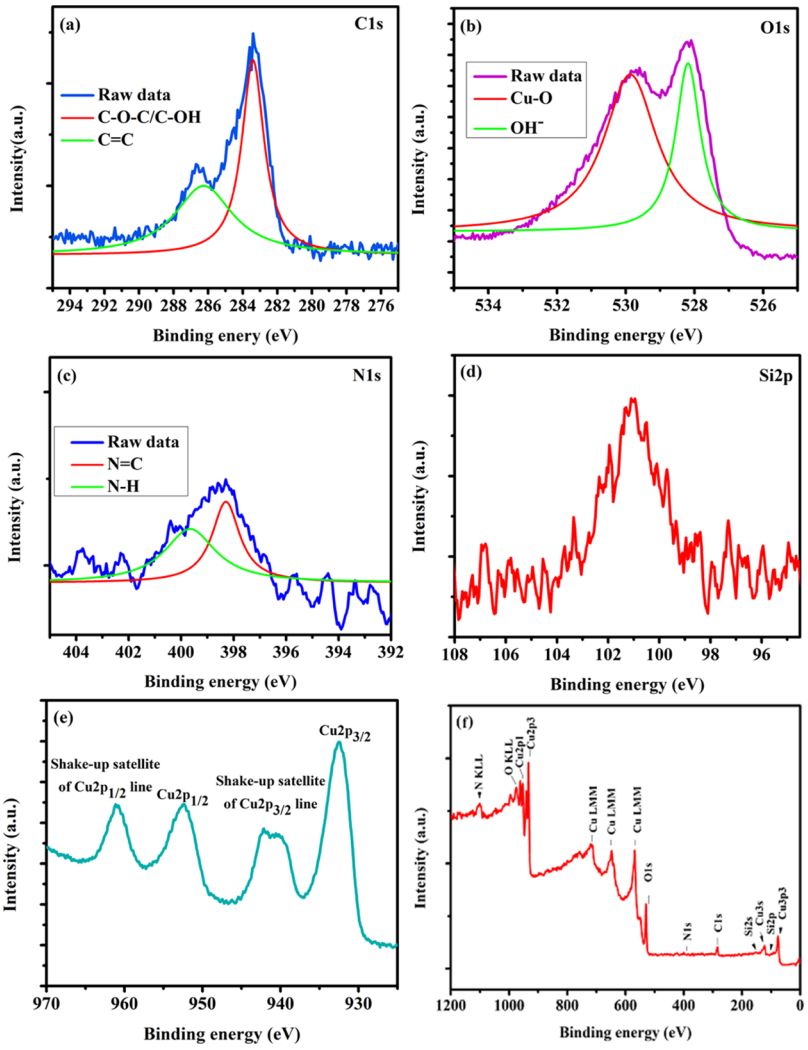

Figure 5. XPS spectra of the Cu(II)-Fur-APTES/GO nanocatalyst, showing peaks representing (a) carbon 1s, (b) oxygen 1s, (c) nitrogen 1s, (d) silicon 2s, (e) Cu(II) and (f) complete scan of the Cu(II)-Fur-APTES/GO nanocatalyst.

Table 1. Optimization of Reaction Conditions[a]

entry	amount of catalyst (mg)	temperature (°C)	time (min)	yield[b] (%)
1	0	50	120	–
2	5	50	120	60
3	10	50	90	75
4	15	50	80	89
5	20	50	30	95
6	20	25	60	78
7	20	40	60	91
8	20	70	30	95
9	30	50	35	95

[a]Reaction conditions: benzaldehyde (1 mmol), dimedone (2 mmol), catalyst (20 mg), solvent (5 mL). [b]Isolated yields.

solvent systems on the percentage yield of xanthenes under different temperature conditions for various time periods. After careful examination of all results water/ethanol mixture in the 1:1 ratio is preferred over other solvents. The ethanol/water (1:1) mixture gave best results. As in case of water, low solubility of aromatic aldehydes and lesser dispersion of the catalyst were prime reasons for lesser activity. Because both water and ethanol are considered as green solvents, so generation of waste from the reaction is minimized and essence of green chemistry is maintained. Thereafter, this particular solvent mixture is used as reaction solvent for all further reactions.

2.5.2. Syntheses of Substituted Xanthene Derivatives Using The Cu(II)-Fur-APTES/GO Nanocatalyst. Using the optimized reaction conditions, we further inspected the opportunity using 5,5-dimethyl-1,3-cyclohexanedione or 1,3-cyclohexanedione (2 mmol), and various benzaldehydes (1 mmol). A wide range of xanthenes are synthesized in good to excellent yield by screening an array of benzaldehydes having electron withdrawing as well as electron donating groups displays Table 2. In case of 4-hydroxy benzaldehyde, longer reaction time would take to complete the reaction which may be because of hydrogen bonding between −OH of aldehyde with the water−ethanol solvent system.

2.6. Plausible Mechanism of the Reaction. Cu(II)-Fur-APTES/GO catalyze synthesis of xanthene derivatives by activating the carbonyl group of aldehydes making it more susceptible to nucleophilic attack by 5,5-dimethyl-1,3-cyclohexanedione to form intermediate (I), followed by Michael addition of another molecule of 5,5-dimethyl-1,3-cyclohexanedione to form the intermediate (II). Intramolecular cyclization occurs after successive elimination of H_2O which

DOI: 10.1021/acsomega.8b01781
ACS Omega 2018, 3, 16377−16385

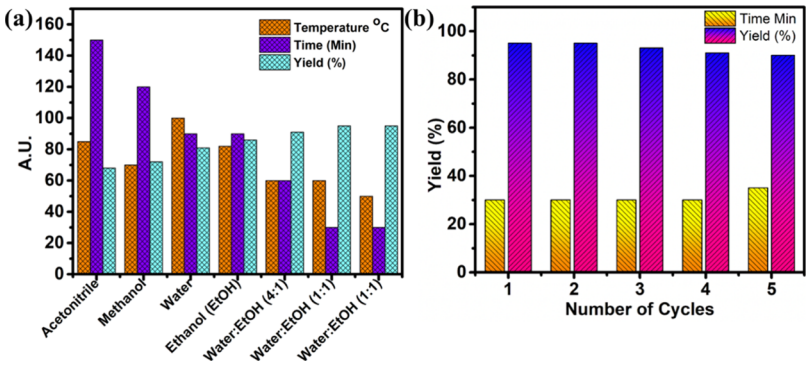

Figure 6. (a) Effect of solvent on percentage yield under same reaction parameters while varying temperature, time, and type of solvent (b) recyclability of the Cu(II)-Fur-APTES/GO nanocatalyst under same reaction conditions of model reaction.

Table 2. Cu(II)-Fur-APTES/GO Catalyzed Synthesis of 1,8-Dioxo-octahydroxanthenes[a]

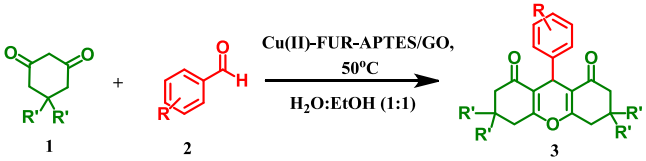

product[c]	R	R′	time (min)	yield[b] (%)
3a	H	CH_3	30	95
3b	3-CH_3	CH_3	35	93
3c	3-Br	CH_3	25	90
3d	3-Cl	CH_3	25	91
3e	3-OCH_3	CH_3	35	90
3f	4-CH_3	CH_3	40	89
3g	4-OCH_3	CH_3	50	89
3h	4-NO_2	CH_3	25	94
3i	4-OH	CH_3	50	86
3j	4-Cl	CH_3	30	92
3k	4-CN	CH_3	30	95
3l	4-Br	CH_3	25	92
3m	H	H	30	94
3n	3-CH_3	H	35	92
3o	3-Br	H	25	94
3p	3-Cl	H	25	91
3q	3-OCH_3	H	35	89
3r	2-CH_3	H	50	85
3s	4-CH_3	H	40	90
3t	4-NO_2	H	30	95

[a]Reaction conditions: aromatic aldehydes (1 mmol), dimedone or 1,3-cyclohexanedione (2 mmol), catalyst (20 mg), solvent (5 mL), temperature 50 °C. [b]Isolated yields. [c]Products were characterized by ^{1}H and ^{13}C NMR spectroscopy.

results in the desired product and regenerates Cu(II)-Fur-APTES/GO in the reaction mixture(Figure 7).

2.7. Comparison of Cu(II)-Fur-APTES/GO with Reported Catalysts for the Synthesis of Xanthenes. A comparison of catalytic efficiency of the Cu(II)-Fur-APTES/GO nanocatalyst with other catalysts, already described in literature, for the preparation of xanthene derivatives, revealed advantages of Cu(II)-Fur-APTES/GO in terms of better yield with shorter reaction time (Table 3, entry 11). In the backdrop of these findings, Cu(II)-Fur-APTES/GO is found to be a very efficient catalyst for efficient synthesis of xanthene and its derivatives (Table 3).

2.8. Recyclability of the Cu(II)-Fur-APTES/GO Nanocatalyst. A highly preferred way to greener and economic synthesis is recovery and recyclability of a catalyst. After endowing the activity and versatility of the Cu(II)-Fur-APTES/GO catalyst for different types of reactions, the recyclability of the catalyst was examined using benzaldehyde and dimedone as model reaction under optimized conditions. The nanocatalyst was separated from the reaction mixture using centrifugation followed by washing with ethyl acetate and ethanol, and finally dried at 80 °C under vacuum for the next cycle of reaction. Recyclability results of the Cu(II)-Fur-APTES/GO nanocatalyst are shown in Figure 6b and tabulated in Table S2. The XRD pattern, Raman spectra and HRTEM images also indicate that the catalyst stability has been maintained up to 5 cycles (Figures 2di,ii and 5d). Hence, it is proving proficiency for various industrial applications.

3. CONCLUSIONS

In summary, a novel, efficient, recyclable, and economic heterogeneous nanocatalyst Cu(II)-Fur-APTES/GO was developed. This nanocatalyst was found as an efficient catalyst for the synthesis of different industry important xanthene and its derivatives under greener solvent conditions with excellent yields. High Cu loading of 13.5 at. % over functionalized GO which is far superior than already known metal-based heterogeneous catalysts which helps in attaining this excellent catalytic performance. Moreover, the recyclability test demonstrated that it can be reused for five consecutive runs without appreciable loss in catalytic efficiency. The additional advantages of the present catalyst include simplicity, reaction time, yield, cost, and selectivity as compared to other catalysts available in literature for the same organic transformation. Furthermore, green solvent condition, ambient reaction conditions, faster synthesis, inexpensive reactants, easy catalyst recovery, and recyclability make this methodology a potential candidate for sustainable synthesis.

4. EXPERIMENTAL SECTION

4.1. Synthesis of GO. GO was synthesized by following the improved synthesis method[67] with some modifications. Briefly, in a round bottom flask, a mixture (9:1) of concd H_2SO_4 and H_3PO_4 was taken, in which 1.5 g of graphite powder was added. After that 9.0 g of $KMnO_4$ was added gradually. The mixture was stirred at 50−55 °C for 12 h. The brown paste so formed was poured into a beaker having ice and subsequently, H_2O_2 (30%, 3 mL) was added to stop the oxidation process which results in the solution turning yellow.

DOI: 10.1021/acsomega.8b01781
ACS Omega 2018, 3, 16377−16385

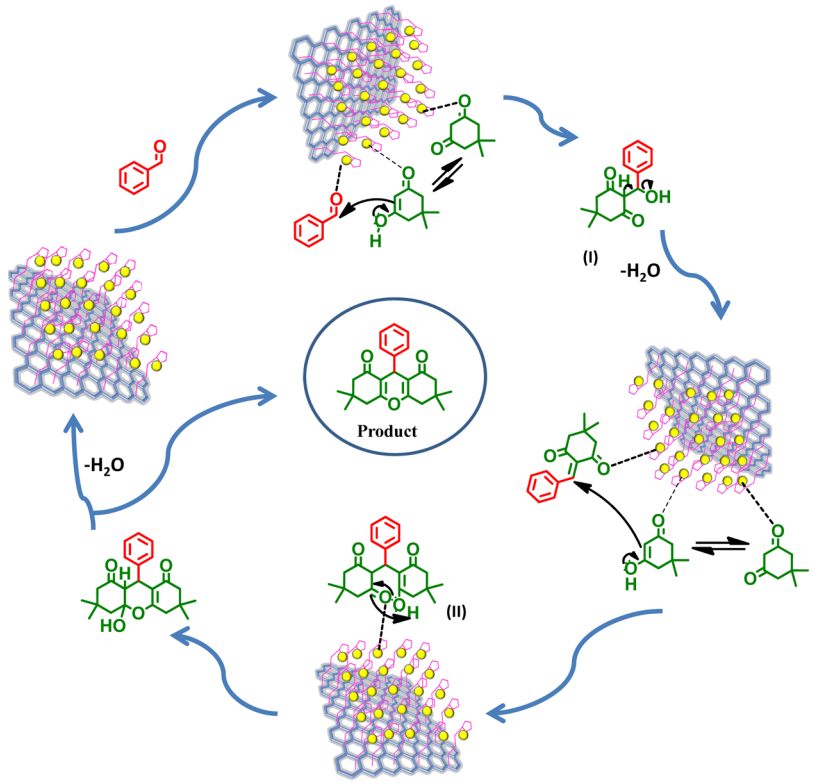

Figure 7. Plausible mechanism for synthesis of xanthenes using the Cu(II)-Fur-APTES/GO nanocatalyst.

Table 3. Comparative Catalytic Performance of the Cu(II)-Fur-APTES/GO Nanocatalyst with Other Previously Reported Catalysts

entry	name of catalyst	amount of catalyst	time/yield (%)	solvent/condition	refs
1	Fe_3O_4@SiO_2-imid-PMAn	30 mg	1.5 h/94	EtOH/reflux	57
2	[bmim]HSO_4	100 mg	3 h/85	solvent free/80 °C	58
3	Fe^{3+}-montmorillonite	85 mg	6 h/94	EtOH/100 °C	14
4	boric acid	0.5 mol %	20 min/98	solvent free/120 °C	59
5	$Zr(DP)_2$	10 mol %	24 h/98	EtOH/reflux	60
6	CuO NPs	7 mg	14 min/89	solvent free/100 °C	61
7	$CaCl_2$	20 mol %	4 h/85	DMSO/85−90 °C	62
8	SO_4^{2-}/ZrO_2	15 wt %	8 h/95	EtOH/70 °C	63
9	p-sulfonic acid calix[4]arene	1.5 mol %	35 min/97	EtOH/80 °C	64
10	SBSSA	30 mg	10 h/98	EtOH/reflux	65
11	ZnO−CH_3COCl	30 mol %	5 h/86	CH_3CN/reflux	66
12	Cu(II)-Fur-APTES/GO	20 mg	30 min/95	H_2O/EtOH (1:1)	present work

Above dispersion was centrifuged and the solid was washed twice with deionized water, followed by washing twice with 30% HCl solution for the removal of undesired metal ions. Then washing with ethanol was carried out repeatedly until a clear brown solid (GO) was obtained.

4.2. Synthesis of Functionalized GO (APTES/GO and Fur-APTES/GO). GO functionalization has been carried out with 3-aminopropyltriethoxysilane (3-APTES). 3-APTES (1.0 mL, 4.28 mmol) was added to 250.0 mL ethanolic solution of well-dispersed GO (250 mg) under vigorous stirring. The mixture was stirred for 20 h at 60 °C under N_2 atmosphere. As the obtained black solid was separated by centrifugation followed by washing with ethanol and dried at 80 °C under vacuum. The isolated black solid was redispersed in ethanol and Fur was added. The reaction mixture was stirred at 60 °C for 24 h. The product was separated using centrifugation, washed with ethanol to remove excess Fur and dried at 80 °C under vacuum. FT-IR approving the formation of imine-functionalized GO is shown in Figure S1.

4.3. Synthesis of GO-Based Copper Nanocatalyst [Cu(II)-Fur-APTES/GO]. To the well-dispersed ethanolic solution of Fur-APTES/GO, copper(II) acetate (2.0 mmol, 0.363 mg) was added and stirred for 24 h at 60 °C. The catalyst was purified by centrifugation, followed by repeated washing with ethanol and drying under vacuum at 80 °C.

4.4. Catalytic Activity. A mixture of aromatic aldehyde (1.0 mmol), 5,5-dimethylcyclohexane-1,3-dione or 1,3-cyclohexanedione (2.0 mmol), Cu(II)-Fur-APTES/GO catalyst (20 mg) in 1:1 aqueous ethanol (5.0 mL) was stirred at 50 °C for suitable time as indicated by thin-layer chromatography. After reaction completion, the reaction mixture was diluted using hot ethanol (10.0 mL) and filtered for catalyst separation. The crude product was obtained by solvent evaporation under reduced pressure and recrystallized from ethanol. The

DOI: 10.1021/acsomega.8b01781
ACS Omega 2018, 3, 16377−16385

recovered catalyst was washed initially with ethyl acetate, afterward with ethanol and dried overnight for further reuse. Recrystallized xanthene derivatives were characterized by ^{1}H and ^{13}C NMR spectroscopy.

NMR spectral data for product 3a, synthesized by model reaction, are given below, while remaining spectroscopic data is provided in Supporting Information.

^{1}H NMR ($CDCl_3$, 400 MHz): δ_H (ppm) 7.28 (d, J = 8.4 Hz, 2H), 7.21 (t, J = 7.6 Hz, 2H), 7.09 (t, J = 7.6 Hz, 1H), 4.75 (s, 1H, CH), 2.46 (s, 4H, 2× CH_2), 2.25−2.14 (m, 4H, 2× CH_2), 1.10 (s, 6H, 2× CH_3), 0.99 (s, 6H, 2× CH_3). ^{13}C NMR (100 MHz, $CDCl_3$): δ_C (ppm) 196.51, 162.37, 144.22, 128.51, 128.18, 126.50, 115.81, 50.87, 41.01, 32.34, 31.96, 29.41, 27.47.

■ ASSOCIATED CONTENT

Supporting Information

The Supporting Information is available free of charge on the ACS Publications website at DOI: 10.1021/acsomega.8b01781.

Materials and characterization techniques, effect of solvent on the catalytic efficiency table; reusability of the Cu(II)-Fur-APTES/GO table; FT-IR spectra; EDX elemental analysis; and ^{1}H and ^{13}C NMR spectra for 3a−3t (PDF)

■ AUTHOR INFORMATION

Corresponding Author

*E-mail: dhanraj_masram27@rediffmail.com. Phone: +91-9958225579 (D.T.M.).

ORCID

Navin Kumar Mogha: 0000-0002-2483-1170

Notes

The authors declare no competing financial interest.

■ ACKNOWLEDGMENTS

Authors are thankful to The Head, Department of Chemistry and Director, University Science Instrumentation Centre (USIC), University of Delhi, Delhi, India for providing instrumentation facilities. Authors are also gratefully acknowledged the Sophisticated Analytical Instrument Facility (SAIF)-AIIMS, New Delhi, under the SAIF Program of DST for providing TEM facility. Subodh, K.C. and G.K. obliged to UGC (University Grants Commission) for providing Junior Research Fellowships.

■ REFERENCES

(1) Khurana, J. M.; Magoo, D.; Aggarwal, K.; Aggarwal, N.; Kumar, R.; Srivastava, C. Synthesis of Novel 12-Aryl-8,9,10,12-Tetrahydrobenzo[a]Xanthene-11-Thiones and Evaluation of Their Biocidal Effects. *Eur. J. Med. Chem.* **2012**, *58*, 470−477.

(2) Hafez, H. N.; Hegab, M. I.; Ahmed-Farag, I. S.; El-Gazzar, A. B. A. A facile regioselective synthesis of novel spiro-thioxanthene and spiro-xanthene-9′,2-[1,3,4]thiadiazole derivatives as potential analgesic and anti-inflammatory agents. *Bioorg. Med. Chem. Lett.* **2008**, *18*, 4538−4543.

(3) Kumar, A.; Rout, L.; Achary, L. S. K.; Dhaka, R. S.; Dash, P. Greener Route for Synthesis of Aryl and Alkyl-14H-Dibenzo [a.j] Xanthenes Using Graphene Oxide-Copper Ferrite Nanocomposite as a Recyclable Heterogeneous Catalyst. *Sci. Rep.* **2017**, *7*, 42975.

(4) Chibale, K.; Visser, M.; van Schalkwyk, D.; Smith, P. J.; Saravanamuthu, A.; Fairlamb, A. H. Exploring the Potential of Xanthene Derivatives as Trypanothione Reductase Inhibitors and Chloroquine Potentiating Agents. *Tetrahedron* **2003**, *59*, 2289−2296.

(5) Jin, T.-S.; Liu, L.-B.; Zhao, Y.; Li, T.-S. Clean Synthesis of Compounds Containing Two 4H-Pyrans or Two Tetraketones in Aqueous Media. *Synth. Commun.* **2005**, *35*, 2379−2385.

(6) Sashidhara, K. V.; Kumar, A.; Dodda, R. P.; Kumar, B. A New Iodine Catalyzed Regioselective Synthesis of Xanthene Synthons. *Tetrahedron Lett.* **2012**, *53*, 3281−3283.

(7) Rajitha, B.; Sunil Kumar, B.; Thirupathi Reddy, Y.; Narsimha Reddy, P.; Sreenivasulu, N. Sulfamic Acid: A Novel and Efficient Catalyst for the Synthesis of Aryl-14H-Dibenzo[a.j]Xanthenes under Conventional Heating and Microwave Irradiation. *Tetrahedron Lett.* **2005**, *46*, 8691−8693.

(8) Khosropour, A.; Khodaei, M.; Moghannian, H. A Facile, Simple and Convenient Method for the Synthesis of 14-Alkyl or Aryl-14-H-Dibenzo[a,j]xanthenes Catalyzed by pTSA in Solution and Solvent-Free Conditions. *Synlett* **2005**, 0955−0958.

(9) Kantevari, S.; Bantu, R.; Nagarapu, L. $HClO_4$-SiO_2 and PPA-SiO_2 catalyzed efficient one-pot Knoevenagel condensation, Michael addition and cyclo-dehydration of dimedone and aldehydes in acetonitrile, aqueous and solvent free conditions: Scope and limitations. *J. Mol. Catal. A: Chem.* **2007**, *269*, 53−57.

(10) Pasha, M. A.; Jayashankara, V. P. Molecular Iodine Catalyzed Synthesis of Aryl-14H-Dibenzo[a, j]Xanthenes under Solvent-Free Condition. *Bioorg. Med. Chem. Lett.* **2007**, *17*, 621−623.

(11) Jin, T.-S.; Zhang, J.-S.; Wang, A.-Q.; Li, T.-S. Solid-State Condensation Reactions Between Aldehydes and 5,5-Dimethyl-1,3-cyclohexanedione by Grinding at Room Temperature. *Synth. Commun.* **2005**, *35*, 2339−2345.

(12) Das, B.; Thirupathi, P.; Reddy, K. R.; Ravikanth, B.; Nagarapu, L. An Efficient Synthesis of 1,8-Dioxo-Octahydroxanthenes Using Heterogeneous Catalysts. *Catal. Commun.* **2007**, *8*, 535−538.

(13) Zhang, Z.-H.; Tao, X.-Y. 2,4,6-Trichloro-1,3,5-Triazine-Promoted Synthesis of 1,8-Dioxo-Octahydroxanthenes under Solvent-Free Conditions. *Aust. J. Chem.* **2008**, *61*, 77−79.

(14) Song, G.; Wang, B.; Luo, H.; Yang, L. Fe^{3+}-Montmorillonite as a Cost-Effective and Recyclable Solid Acidic Catalyst for the Synthesis of Xanthenediones. *Catal. Commun.* **2007**, *8*, 673−676.

(15) Venkatesan, K.; Pujari, S. S.; Lahoti, R. J.; Srinivasan, K. V. An Efficient Synthesis of 1,8-Dioxo-Octahydro-Xanthene Derivatives Promoted by a Room Temperature Ionic Liquid at Ambient Conditions under Ultrasound Irradiation. *Ultrason. Sonochem.* **2008**, *15*, 548−553.

(16) Pourian, E.; Javanshir, S.; Dolatkhah, Z.; Molaei, S.; Maleki, A. Ultrasonic-Assisted Preparation, Characterization, and Use of Novel Biocompatible Core/Shell Fe_3O_4@GA@Isinglass in the Synthesis of 1,4-Dihydropyridine and 4H-Pyran Derivatives. *ACS Omega* **2018**, *3*, 5012−5020.

(17) Karimi-Jaberi, Z.; Keshavarzi, M. Efficient One-Pot Synthesis of 14-Substituted-14H-Dibenzo[a,j]Xanthenes Using Boric Acid under Solvent-Free Conditions. *Chin. Chem. Lett.* **2010**, *21*, 547−549.

(18) Xia, Y.; Yang, H.; Campbell, C. T. Nanoparticles for Catalysis. *Acc. Chem. Res.* **2013**, *46*, 1671−1672.

(19) Sydnes, M. Use of Nanoparticles as Catalysts in Organic Synthesis - Cross-coupling Reactions. *Curr. Org. Chem.* **2014**, *18*, 312−326.

(20) Fan, X.; Zhang, G.; Zhang, F. Multiple Roles of Graphene in Heterogeneous Catalysis. *Chem. Soc. Rev.* **2015**, *44*, 3023−3035.

(21) Geim, A. K.; Novoselov, K. S. The Rise of Graphene. *Nat. Mater.* **2007**, *6*, 183−191.

(22) Sharma, D.; Kanchi, S.; Sabela, M. I.; Bisetty, K. Insight into the Biosensing of Graphene Oxide: Present and Future Prospects. *Arab. J. Chem.* **2016**, *9*, 238−261.

(23) Khan, M.; Al-Marri, A. H.; Khan, M.; Shaik, M. R.; Mohri, N.; Adil, S. F.; Kuniyil, M.; Alkhathlan, H. Z.; Al-Warthan, A.; Tremel, W.; et al. Green Approach for the Effective Reduction of Graphene Oxide Using Salvadora Persica L. Root (Miswak) Extract. *Nanoscale Res. Lett.* **2015**, *10*, 987.

DOI: 10.1021/acsomega.8b01781
ACS Omega 2018, 3, 16377−16385

(24) Singh, V. V.; Singh, A. K. Nanoflowers of $Cu_{1.8}S$: Free and Decorated on Graphene Oxide (GO-$Cu_{1.8}S$) as Efficient and Recyclable Catalysts for C-O Coupling. *ACS Appl. Nano Mater.* **2018**, *1*, 2164−2174.
(25) Dong, S.; Liu, Z.; Liu, R.; Chen, L.; Chen, J.; Xu, Y. Visible-Light-Induced Catalytic Transfer Hydrogenation of Aromatic Aldehydes by Palladium Immobilized on Amine-Functionalized Iron-Based Metal-Organic Frameworks. *ACS Appl. Nano Mater.* **2018**, *1*, 4247−4257.
(26) Lonkar, S. P.; Pillai, V. V.; Alhassan, S. M. Three-Dimensional NiS-MoS_2/Graphene Heterostructured Nanohybrids as High-Performance Hydrodesulfurization Catalysts. *ACS Appl. Nano Mater.* **2018**, *1*, 3114−3123.
(27) Zhang, M.; Liu, Y.-H.; Shang, Z.-R.; Hu, H.-C.; Zhang, Z.-H. Supported molybdenum on graphene oxide/Fe_3O_4: An efficient, magnetically separable catalyst for one-pot construction of spirooxindole dihydropyridines in deep eutectic solvent under microwave irradiation. *Catal. Commun.* **2017**, *88*, 39−44.
(28) Iqbal, M.; Li, C.; Jiang, B.; Hossain, M. S. A.; Islam, M. T.; Henzie, J.; Yamauchi, Y. Tethering Mesoporous Pd Nanoparticles to Reduced Graphene Oxide Sheets Forms Highly Efficient Electrooxidation Catalysts. *J. Mater. Chem. A* **2017**, *5*, 21249−21256.
(29) Mogha, N. K.; Kirti, S.; Masram, D. T. La_2O_3/Reduced Graphene Oxide Nanocomposite: A Highly Efficient, Reusable Heterogeneous Catalyst for the Synthesis of Biologically Important Bis(Indolyl)Methanes Under Solvent Free Conditions. *J. Nanosci. Nanotechnol.* **2017**, *17*, 2508−2514.
(30) Ahuja, P.; Ujjain, S. K.; Arora, I.; Samim, M. Hierarchically Grown NiO-Decorated Polyaniline-Reduced Graphene Oxide Composite for Ultrafast Sunlight-Driven Photocatalysis. *ACS Omega* **2018**, *3*, 7846−7855.
(31) Tatykayev, B.; Donat, F.; Alem, H.; Balan, L.; Medjahdi, G.; Uralbekov, B.; Schneider, R. Synthesis of Core/Shell ZnO/RGO Nanoparticles by Calcination of ZIF-8/RGO Composites and Their Photocatalytic Activity. *ACS Omega* **2017**, *2*, 4946−4954.
(32) Park, J.; Jin, T.; Liu, C.; Li, G.; Yan, M. Three-Dimensional Graphene-TiO_2 Nanocomposite Photocatalyst Synthesized by Covalent Attachment. *ACS Omega* **2016**, *1*, 351−356.
(33) Pumera, M. Graphene-Based Nanomaterials for Energy Storage. *Energy Environ. Sci.* **2011**, *4*, 668−674.
(34) Chen, X.-M.; Wu, G.-H.; Chen, J.-M.; Jiang, Y.-Q.; Chen, G.-N.; Oyama, M.; Chen, X.; Wang, X.-R. A novel electrochemiluminescence sensor based on bis(2,2′-bipyridine)-5-amino-1,10-phenanthroline ruthenium(II) covalently combined with graphite oxide. *Biosens. Bioelectron.* **2010**, *26*, 872−876.
(35) Mogha, N. K.; Sahu, V.; Sharma, M.; Sharma, R. K.; Masram, D. T. Biocompatible ZrO_2—reduced graphene oxide immobilized AChE biosensor for chlorpyrifos detection. *Mater. Des.* **2016**, *111*, 312−320.
(36) Mogha, N. K.; Sahu, V.; Sharma, M.; Sharma, R. K.; Masram, D. T. Sensitive and Reliable Ascorbic Acid Sensing by Lanthanum Oxide/Reduced Graphene Oxide Nanocomposite. *Appl. Biochem. Biotechnol.* **2014**, *174*, 1010−1020.
(37) Tozzini, V.; Pellegrini, V. Prospects for Hydrogen Storage in Graphene. *Phys. Chem. Chem. Phys.* **2013**, *15*, 80−89.
(38) Liu, Z.; Robinson, J. T.; Sun, X.; Dai, H. PEGylated Nanographene Oxide for Delivery of Water-Insoluble Cancer Drugs. *J. Am. Chem. Soc.* **2008**, *130*, 10876−10877.
(39) Shen, H.; Zhang, L.; Liu, M.; Zhang, Z. Biomedical Applications of Graphene. *Theranostics* **2012**, *2*, 283−294.
(40) Liu, C.; Yu, Z.; Neff, D.; Zhamu, A.; Jang, B. Z. Graphene-Based Supercapacitor with an Ultrahigh Energy Density. *Nano Lett.* **2010**, *10*, 4863−4868.
(41) Salunkhe, R. R.; Hsu, S.-H.; Wu, K. C. W.; Yamauchi, Y. Large-Scale Synthesis of Reduced Graphene Oxides with Uniformly Coated Polyaniline for Supercapacitor Applications. *ChemSusChem* **2014**, *7*, 1551−1556.
(42) Mogha, N. K.; Gosain, S.; Masram, D. T. Gold Nanoworms Immobilized Graphene Oxide Polymer Brush Nanohybrid for Catalytic Degradation Studies of Organic Dyes. *Appl. Surf. Sci.* **2017**, *396*, 1427−1434.
(43) Mogha, N. K.; Gosain, S.; Masram, D. T. Lanthanum Oxide Nanoparticles Immobilized Reduced Graphene Oxide Polymer Brush Nanohybrid for Environmental Vitiation of Organic Dyes. *Arab. J. Chem.* **2017**, DOI: 10.1016/j.arabjc.2017.11.008.
(44) Sharma, R. K.; Dutta, S.; Sharma, S.; Zboril, R.; Varma, R. S.; Gawande, M. B. Fe_3O_4 (iron oxide)-supported nanocatalysts: synthesis, characterization and applications in coupling reactions. *Green Chem* **2016**, *18*, 3184−3209.
(45) Lam, E.; Luong, J. H. T. Carbon Materials as Catalyst Supports and Catalysts in the Transformation of Biomass to Fuels and Chemicals. *ACS Catal* **2014**, *4*, 3393−3410.
(46) Baig, R. B. N.; Varma, R. S. Magnetically Retrievable Catalysts for Organic Synthesis. *Chem. Commun.* **2013**, *49*, 752−770.
(47) Mondal, J.; Modak, A.; Dutta, A.; Basu, S.; Jha, S. N.; Bhattacharyya, D.; Bhaumik, A. One-Pot Thioetherification of Aryl Halides with Thiourea and Benzyl Bromide in Water Catalyzed by Cu-Grafted Furfural Imine-Functionalized Mesoporous SBA-15. *Chem. Commun.* **2012**, *48*, 8000−8002.
(48) Khan, S.; Ansari, A. A.; Khan, A. A.; Abdulla, M.; Al-Obaid, O.; Ahmad, R. In Vitro Evaluation of Cytotoxicity, Possible Alteration of Apoptotic Regulatory Proteins, and Antibacterial Activity of Synthesized Copper Oxide Nanoparticles. *Colloids Surf., B* **2017**, *153*, 320−326.
(49) Su, H.; Li, Z.; Huo, Q.; Guan, J.; Kan, Q. Immobilization of Transition Metal (Fe^{2+}, Co^{2+}, VO^{2+} or Cu^{2+}) Schiff Base Complexes onto Graphene Oxide as Efficient and Recyclable Catalysts for Epoxidation of Styrene. *RSC Adv.* **2014**, *4*, 9990−9996.
(50) Zhao, Q.; Bai, C.; Zhang, W.; Li, Y.; Zhang, G.; Zhang, F.; Fan, X. Catalytic Epoxidation of Olefins with Graphene Oxide Supported Copper (Salen) Complex. *Ind. Eng. Chem. Res.* **2014**, *53*, 4232−4238.
(51) Huang, Q.; Zhou, L.; Jiang, X.; Zhou, Y.; Fan, H.; Lang, W. Synthesis of Copper Graphene Materials Functionalized by Amino Acids and Their Catalytic Applications. *ACS Appl. Mater. Interfaces* **2014**, *6*, 13502−13509.
(52) Bahrami, K.; Sheikh Arabi, M. Copper Immobilized Ferromagnetic Nanoparticle Triazine Dendrimer (FMNP@TD-Cu(Ii))-Catalyzed Regioselective Synthesis of 1,4-Disubstituted 1,2,3-Triazoles. *New J. Chem.* **2016**, *40*, 3447−3455.
(53) Kumar, S.; Kumar, P.; Jain, S. L. Graphene oxide immobilized copper phthalocyanine tetrasulphonamide: the first heterogenized homogeneous catalyst for dimethylcarbonate synthesis from CO_2 and methanol. *J. Mater. Chem. A* **2014**, *2*, 18861−18866.
(54) Hajipour, A. R.; Jajarmi, S. Highly efficient and reusable polystyrene-supported copper(II) catalytic system for S-arylation of potassium thiocyanate by aryl halides in water. *Appl. Organomet. Chem.* **2016**, *30*, 566−570.
(55) Naeimi, H.; Shaabani, R.; Moradian, M. Functionalized Graphene Oxide Supported Copper (I) Complex as Effective and Recyclable Nanocatalyst for One-Pot Three Component Synthesis of 1,2,3-Triazoles. *Appl. Organomet. Chem.* **2017**, *31*, No. e3626.
(56) Sun, J.; Kan, Q.; Li, Z.; Yu, G.; Liu, H.; Yang, X.; Huo, Q.; Guan, J. Different Transition Metal (Fe^{2+}, Co^{2+}, Ni^{2+}, Cu^{2+} or VO^{2+}) Schiff Complexes Immobilized onto Three-Dimensional Mesoporous Silica KIT-6 for the Epoxidation of Styrene. *RSC Adv.* **2014**, *4*, 2310−2317.
(57) Esmaeilpour, M.; Javidi, J.; Dehghani, F.; Nowroozi Dodeji, F. Fe_3O_4@SiO_2-imid-PMAn magnetic porous nanospheres as recyclable catalysts for the one-pot synthesis of 14-aryl- or alkyl-14H-dibenzo[a,j]xanthenes and 1,8-dioxooctahydroxanthene derivatives under various conditions. *New J. Chem.* **2014**, *38*, 5453−5461.
(58) Niknam, K.; Damya, M. 1-Butyl-3-methylimidazolium Hydrogen Sulfate [Bmim]HSO_4: An Efficient Reusable Acidic Ionic Liquid for the Synthesis of 1,8-Dioxo-Octahydroxanthenes. *J. Chin. Chem. Soc.* **2009**, *56*, 659−665.
(59) Rezayati, S.; Hajinasiri, R.; Erfani, Z.; Rezayati, S.; Afshari-sharifabad, S. Boric Acid as a Highly Efficient and Reusable Catalyst

DOI: 10.1021/acsomega.8b01781
ACS Omega 2018, 3, 16377−16385

for the One-Pot Synthesis of 1,8-Dioxo-Octahydroxanthenes under Solvent-Free Conditions. *Iran. J. Catal.* **2014**, *4*, 157−162.
(60) Ghassamipour, S.; Ghashghaei, R. Zirconium dodecylphosphonate promoted synthesis of xanthene derivatives by condensation reaction of aldehydes and β-naphthol or dimedone in green media. *Monatsh. Chem.* **2015**, *146*, 159−163.
(61) Chaudhary, G. R.; Bansal, P.; Kaur, N.; Mehta, S. K. Recyclable CuO Nanoparticles as Heterogeneous Catalysts for the Synthesis of Xanthenes under Solvent Free Conditions. *RSC Adv.* **2014**, *4*, 49462−49470.
(62) Ilangovan, A.; Muralidharan, S.; Sakthivel, P.; Malayappasamy, S.; Karuppusamy, S.; Kaushik, M. P. Simple and Cost Effective Acid Catalysts for Efficient Synthesis of 9-Aryl-1,8-Dioxooctahydroxanthene. *Tetrahedron Lett* **2013**, *54*, 491−494.
(63) Kahandal, S. S.; Burange, A. S.; Kale, S. R.; Prinsen, P.; Luque, R.; Jayaram, R. V. An Efficient Route to 1,8-Dioxo-Octahydroxanthenes and -Decahydroacridines Using a Sulfated Zirconia Catalyst. *Catal. Commun.* **2017**, *97*, 138−145.
(64) Baghbanian, S. M.; Khanzad, G.; Vahdat, S. M.; Tashakkorian, H. P-Sulfonic Acid Calix[4]Arene as an Efficient and Reusable Catalyst for the Synthesis of Acridinediones and Xanthenes. *Res. Chem. Intermed.* **2015**, *41*, 9951−9966.
(65) Niknam, K.; Panahi, F.; Saberi, D.; Mohagheghnejad, M. Silica-Bonded *S* -Sulfonic Acid as Recyclable Catalyst for the Synthesis of 1,8-Dioxo-Decahydroacridines and 1,8-Dioxo-Octahydroxanthenes. *J. Heterocycl. Chem.* **2010**, *47*, 292−300.
(66) Maghsoodlou, M. T.; Habibi-Khorassani, S. M.; Shahkarami, Z.; Maleki, N.; Rostamizadeh, M. An efficient synthesis of 2,2′-arylmethylene bis(3-hydroxy-5,5-dimethyl-2-cyclohexene-1-one) and 1,8-dioxooctahydroxanthenes using ZnO and ZnO-acetyl chloride. *Chin. Chem. Lett.* **2010**, *21*, 686−689.
(67) Marcano, D. C.; Kosynkin, D. V.; Berlin, J. M.; Sinitskii, A.; Sun, Z.; Slesarev, A.; Alemany, L. B.; Lu, W.; Tour, J. M. Improved Synthesis of Graphene Oxide. *ACS Nano* **2010**, *4*, 4806−4814.

DOI: 10.1021/acsomega.8b01781
ACS Omega 2018, 3, 16377−16385